A 2 MW grid-tied fuel cell inverter under a single loop control scheme

Doudou N. Luta
Mechatronics Engineering Department
Cape Peninsula University of Technology
Cape Town, South Africa
lutad@cput.ac.za

Atanda K. Raji
Electrical Engineering Department
Cape Peninsula University of Technology
Cape Town, South Africa
rajia@cput.ac.za

***Abstract*— Distributed energy resources are significant players in the shift from fossil fuel to green energy systems. Because these power-generating units are increasingly being integrated into existing utility grids, ordinary consumers are now active stakeholders, referred to as prosumers. Their capabilities are not limited to consuming electricity but also generating and storing it. A change in electricity consumption flexibility has emerged from introducing the energy prosumer idea and the structural shift in the energy sector. That's because if the generation capacity of a prosumer exceeds the load connected to its terminals, there will be a considerable amount of excess electricity. In this case, the prosumer can use the Peer-to-Peer electricity trading mechanism to sell the excess electricity to neighbouring loads or the utility grid. This work deals with controlling a grid-tied 2 MW fuel cell prosumer. The goal is to simulate the system with the inverter operating under the single loop PQ control scheme. A phase-locked-loop is employed to synchronize the fuel cell inverter's frequency and phase with the grid corresponding parameters. Harmonics are mitigated using an LC filter that interfaces the inverter and the grid. The simulation is carried out in Matlab/Simulink environment.**

Keywords— Alternative energy, Fuel Cell, Multilevel Inverter, VOC PQ control.

I. INTRODUCTION

Distributed energy resources are key elements in migrating from fossil fuel to green energy [1]. Their ever-rising integration into pre-existing grids has permitted ordinary consumers to become active stakeholders, referred to as prosumers [2]. Their capabilities are not limited to consuming electricity but also generating and storing it. A change in electricity consumption flexibility has emerged from introducing the energy prosumer idea and the structural shift in the energy sector. That's because if the generation capacity of a prosumer exceeds the load connected to its terminals, there will be a considerable amount of excess electricity. In this instance, the prosumer can use the Peer-to-Peer electricity trading mechanism to sell the excess electricity to neighbouring loads or the utility grid. Prosumers also contribute to smart grids running by offering utility grids with supplementary services.

In South Africa, for example, the electricity business model is extremely unidirectional; The country public utility (Eskom) produces, distributes, and sells electricity to industrial, commercial, and residential customers, either independently or through municipal entities. According to Kane [3], as businesses emerge from the COVID-19-lockdown into an environment still weakened by the prospect of load-shedding and energy cost increases, plenty will likely consider moving to off-grid units or searching for ways to supplement their power requirements with renewable energies. This will enable a huge shift, with the power network and grid evolving to the point where individuals or businesses can export or import energy to the system. People who have photovoltaic panels installed at their homes are thought to be the most likely prosumers. However, more big users, such as manufacturing corporations, are anticipated to follow suit.

This study covers a grid-tied solid oxide fuel cell prosumer with a capacity of 2 megawatts. The voltage generated in a normal fuel cell is inherently unstable because it depends entirely on the load and fuel intake. In most cases, delivering electricity to a load from a fuel cell necessitates the use of a power electronic converter. It balances, improves, and converts DC electricity into AC power effectively. The widespread usage of large-scale power converters in grid-tied fuel cells can substantially impact grid stability and performance and power quality. As a result, adequate control configurations of these inverters are imperative to prevent these problems and assure the correct operation of the system.

Inverter control is divided into three stages: external control loop for the active/reactive power control, current control loop, and synchronization [4]. To inject the required active/reactive powers, the current controller monitors the reference-current generated by the active/reactive power controller. The grid information required in the control loops is extracted during the synchronization stage. In most cases, a PLL is utilized to retrieve the grid data. Its major responsibility is to provide a unit power factor, which entails the synchronization of the inverter current with the grid voltage while supplying a smooth sinusoidal reference-current [4].

A filter interconnects the inverter terminals and the grid in order to minimize harmonics impacts and adhere to harmonic control regulations. An LC passive filter is selected in this study because of its simplicity.

The control of a 2 MW grid-tied fuel cell inverter is the subject of this research. The goal is to simulate the system with the inverter operating under the single loop active and reactive power control scheme. A phase-locked-loop synchronizes the inverter's phase and frequency with the grid corresponding parameters. Harmonics are mitigated using an LC filter that interfaces the inverter and the grid. The simulation is carried out in Matlab/Simulink environment.

The remainder of the article is arranged as follows: in Section II, the adopted system is modeled, in Section III, the simulation results are shown, and in Section IV, concluding thoughts are presented.

978-1-6654-6887-9/22/$31.00 ©2022 IEEE

II. Grid-Tied Fuel Cell Configuration and Modeling

A fuel cell stack, a three-phase three-level diode-clamped inverter, and an LC filter that connects a solid-oxide fuel cell stack to the grid are depicted in Figure 1. The fuel cell plant produces 2 MW at 2000 Vdc, while the inverter produces 1.73 MW AC at 415 V for the grid since its adopted power factor is 0.865.

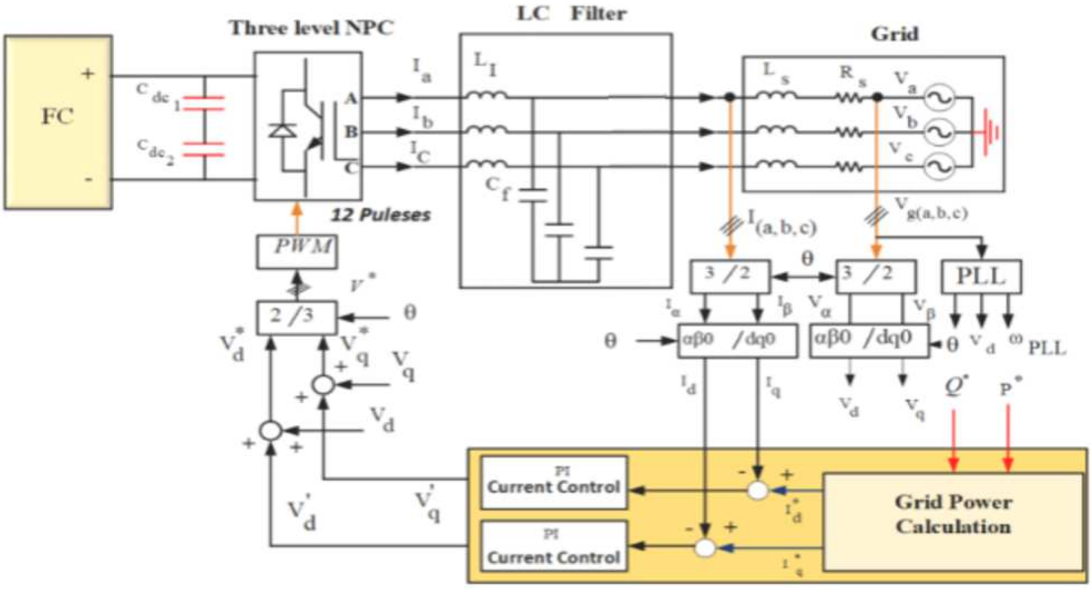

Fig. 1. Grid-tied fuel cell under a single loop control scheme layout. [5]

A. Fuel Cell

The equation below defines the dynamic fuel model [4]:

$$V_{FC} = E - V_{act} - V_{ohm} - V_{conc} \quad (1)$$

Where V_{FC} is the fuel cell, E represents the Nernst, V_{act} is the activation-voltage, V_{conc} is the concentration-voltage, and V_{ohm} the ohmic-losses; these are respectively defined in Equations. 2 - 6.

$$E = E_0 + \frac{RT}{4F} ln \left[\frac{(pH_2)^2 .\ pO_2}{(pH_2o)^2}\right] \quad (2)$$

$$V_{act} = \frac{RT}{n\alpha F} ln \left(I_{fc}/2I_0 + \sqrt{(I_{fc}/2I_0)^2 + 1} \right) \quad (3)$$

$$I_{fc} = I_0 \left(e^{(\alpha_1 F/RT)V_{act} - e^{(\alpha_2 F/RT)V_{act}}} \right) \quad (4)$$

$$V_{conc} = -\frac{RT}{nF} ln \left[1 - \frac{I_{fc}}{I_L} \right] \quad (5)$$

$$V_{ohmic} = \left(\gamma\ exp \left[\beta \left(\frac{1}{T_0} - \frac{1}{T} \right) \right] \right) I_{fc} = r I_{fc} \quad (6)$$

With γ and β being the fuel cell constant coefficients, T_0 =973 °K, T is the working temp. of the fuel cell, r is the internal resistance, while E_0 represents the standard potential which is equal to 1.18 V; R stands for the gas constant, F, pH_2, pO_2, and pH_2O are the Faraday constant, the hydrogen partial, oxygen, and water effective gas partial pressures, respectively, I_L represents the cell maximum current density at a specific flow rate, and I_0 the fuel cell apparent exchange current.

The fuel cell modeling parameters are given in Table I.

TABLE I. Fuel Cell Parameters

Solid-oxide fuel cell parameters	
Parameter	***Value***
Initial current	1000 Amperes
Ideal standards potential	1.18 Volts
Total cells	2810
Operating voltage	2000 Volts
Cell ohmic loss	3.2813e-4 ohms
Optimal, maximum, minimum and fuel utilization	[0.85 0.9 0.8]
Hydrogen, oxygen, and water valve molar constant	[8.43e-4 2.52e-3 2.81e-4] kmol/s atm
Absolutte temperature	1273^0 K
Faraday's constant	96.487e6

B. NPC inverter

Clamping diodes and cascaded DC capacitors are used in the three-level diode-clamped (NPC) inverter to generate nearly sinusoidal three-level AC waves. The operation is conducted at a low switching frequency, with only moderate filtering needs and negligible harmonic distortion [6], [7]. The switching process of switching devices produces the three-level inverter output voltage. As depicted in Table II, given the switches S_{a1}, S_{a2}, S_{a3} and S_{a4}, when S_{a1} and S_{a2} are in on position and S_{a3} and S_{a4} are in off position, the inverter AC output voltage is $V_{dc}/2$. On the contrary, the AC voltage is -$V_{dc}/2$. When S_{a1} and S_{a4} are in off position and S_{a2} and S_{a3} are in on position, the AC output voltage is nil [8], [9]. The inverter design parameters are given in Table III.

TABLE II. NPC INVERTER STATES

State table					
Changing State	**Switch states**				**Output**
State	Sa1	Sa2	Sa3	Sa4	Voltage
P	ON	ON	OFF	OFF	+Vdc/2
O	OFF	OFF	ON	OFF	0
N	OFF	OFF	ON	ON	-Vdc/2

TABLE III. NPC INVERTER DESIGN FEATURES

Parameter	Value and unit
DC output power	2 megawatts
DC-link voltage	2000 Volts
Inverter AC power	1.73 megawatts
AC voltage before filtering (Line-to-line)	1400 Volts
AC voltage after filtering (Line-to-line)	415 Volts
Phase current measured after filter	373.4 Amperes
Power factor	0.85
Line current	528.1 Amperes
Switching-frequency	7000 Hertz
Grid-frequency	50 Hertz
Attenuation-factor	20 %
Grid maximal power factor change	5 %
Inverter-configuration	Three-phase

C. PQ control approach

The active & reactive feed-forward power control and a current regulator in the dq0 frame are used in the control scheme. The DC voltage control actualizes the active and reactive reference power control; this necessitates converting the reactive and active power command signals into d and q components of the reference-current using the matrix presented as [5]:

$$\begin{bmatrix} i_d^* \\ i_q^* \end{bmatrix} = \frac{1}{v_{gd}^2+v_{gq}^2}\begin{bmatrix} v_{gd} & -v_{gq} \\ v_{gq} & v_{gd} \end{bmatrix}\begin{bmatrix} P^* \\ Q^* \end{bmatrix} \tag{7}$$

This study adopted active and reactive power references are 1.73 MW and 0 VAR, respectively. The adopted active power refers to the active power of the inverter.

Current control

The d and q axis control loops in the current control share comparable features. As a result of the equivalency of the q axis parameters, the tuning of the PI controller is restricted to the d axis. The feed-forward voltage and decoupling between the d and q axes are labeled as disturbances (Figure 2); thus, they are ignored [10].

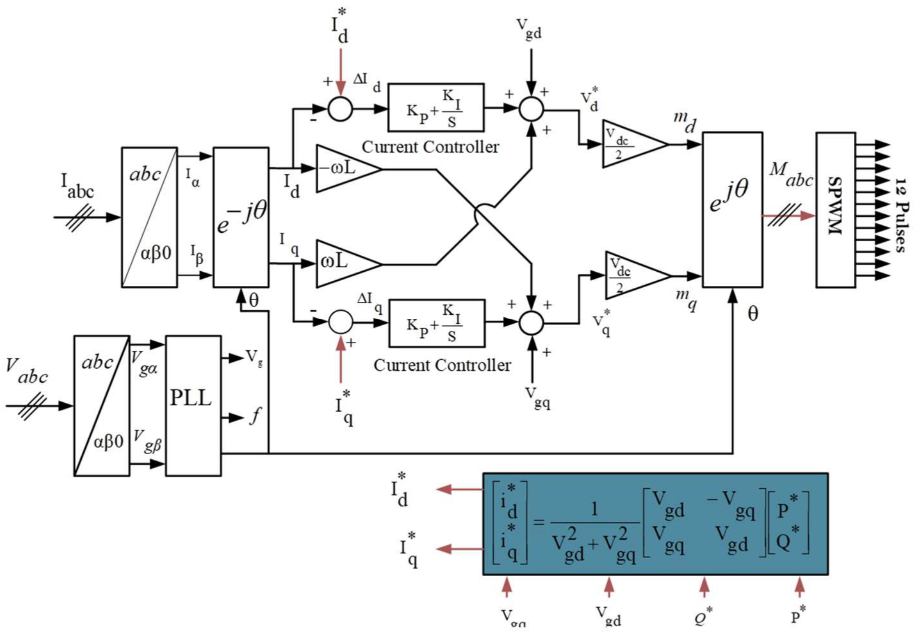

Fig. 2. Single loop control scheme diagram [5]

The current loop in Figure 3 has the following transfer function:

$$H_{cu} = H_{PI} \times H_C \times H_{INV} \times H_{LCL} \times H_S \tag{8}$$

The loop's simplified transfer function is given as [5]:

$$H_{cu} = \frac{k_p s+k_i}{s}\,\frac{1}{1+s(T_S+0.5T_{SW}+0.5T_S)}\,\frac{\frac{1}{R}}{\left[s\left(\frac{L}{R}\right)+1\right]} \tag{9}$$

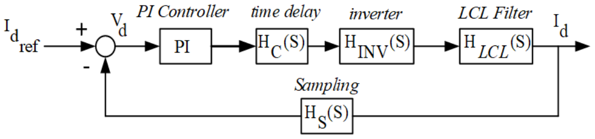

Fig. 3. Current loop block diagram

From Equation 9, K_p and K_i are obtained as follows [5]:

$$K_p = \frac{5L}{2T_S} \quad (10)$$

$$K_i = \frac{k_p}{\frac{L}{R}} \quad (11)$$

D. PLL (Phase-locked loop)

A PI controller (loop filter), Clarke & Park transformations, and a voltage-controlled oscillator (VCO) (integrator) are all included in the dq0 frame representation of a PLL [11]. Equation 12 expresses the PLL transfer function $H(s)$, which is identical to Equation 13's second-order system transfer function $G(s)$ [12].

$$H(s) = \frac{k_{p\_pll}s + k_{i\_pll}}{s^2 + k_{p\_pll}s + k_{i-pll}} \quad (12)$$

$$G(s) = \frac{2\zeta\omega_n s + \omega_n^2}{s^2 + 2\zeta\omega_n s + \omega_n^2} \quad (13)$$

where k_{p_pll} is the PLL proportional gain and and k_{i_pll} is the PLL integral gain; ω_n is the natural frequency, while ζ represents the damping ratio. Based on Equations 14 and 15, k_{p_pll} and k_{i_pll} are given as follows:

$$k_{i\_pll} = \omega_n^2 \quad (14)$$

$$k_{p\_pll} = 2\zeta\sqrt{k_{i\_pll}} \quad (15)$$

Table IV provides the gains K_p, K_i, k_{p_pll} and k_{i_pll} of the control scheme.

TABLE IV. PQ CONTROL PARAMETERS

Parameters	
Power references	
Active power	1.73 megawatts
Reactive power	0 VAR
Current controller	
Proportional gain (K_p)	12.08
Integral gain (K_i)	185.8
PLL	
Controller Proportional gain (k_{p_pll})	15.9
Controller Integral gain (k_{i_pll})	69130.43

E. LC filter design

The input parameters required for the LC filter design include the inverter rated power P_{rated}, the DC-bus voltage V_{DC}, the switching, sampling, and grid frequencies f_g, f_s and f_{sw}, respectively, and the grid voltage V_g. Table VI presents the designed parameters of the LC filter achieved by determining the critical & resonance frequencies and the correlation constant; later, the capacitor, the grid-side & inverter-side inductances, the ripple, and the damping resistor were determined.

Critical frequency

The following equations define the critical frequency ω_{crit} (f_{crit}):

$$\omega_{crit} = \pi/3T_s \quad (16)$$

$$f_{crit} = \frac{\pi}{3} f_s \frac{1}{2\pi} = f_s/6 \quad (17)$$

Where ω_{crit} (f_{crit}) is the critical frequency, and T_s the sampling period.

Resonance frequency

Equation 18 gives the expression of the resonance frequency f_{res} as follows:

$$f_{res}/f_s = 0.10\sim0.12 \quad (18)$$

Moreover, the inequality in Equation 19 must always be satisfied.

$$10f_g < f_{res} < 0.5f_{sw} \quad (19)$$

Capacitor

Equation 20 gives the capacitor value:

$$C_f = x \times \frac{P_{rated}}{3\times 2\pi \times f_g \times V_g^2} \quad (20)$$

where x is the rate of reactive power absorption, which can range from 0.01 to 0.05 [13].

Inductance

The inductance can be calculated using the formula below:

$$f_{res} = \frac{1}{2\pi}\sqrt{\frac{1}{L_c C_f}} \quad (21)$$

Current ripple

The current ripple (Δi) is given in Equation 22 as follows [14].

$$\Delta i = \frac{V_{dc}}{8L_c f_{sw}} \leq \left(\frac{Ripple\%}{100}\right) \times \hat{I}_f \quad (22)$$

Δi; the ripple current must not exceed 10 to 25% of the rated peak current $\hat{I}_f$[15].

TABLE V. LC FILTER PARAMETERS

Parameter	Value and unit
Inductance	2.5 milli Henry
Capacitor	518 micro Farads
Resonance-frequency	2865.77 Hertz
Inductor resistances	0.014 ohm
Sampling-frequency	20000 Hertz
Critical=frequency	859.7 Hertz

III. SIMULATION RESULTS AND DISCUSSION

To evaluate its performance, the grid-tied 2 MW fuel cell unit, shown in Figure 1, was modeled and simulated in the Matlab/Simelectrical environment. The parameters from Tables I, II, IV, and V are used, and the results reveal that the developed controller performs well.

Figure 4 shows the output power and voltage of a fuel cell. The fuel cell has a capacity of 2MW and a voltage of 2 kV. The current generated is 1000 A. To facilitate grid connection while supplying electricity to a local AC load, the DC voltage and current (DC power) at the output of the fuel cell stack are converted to AC.

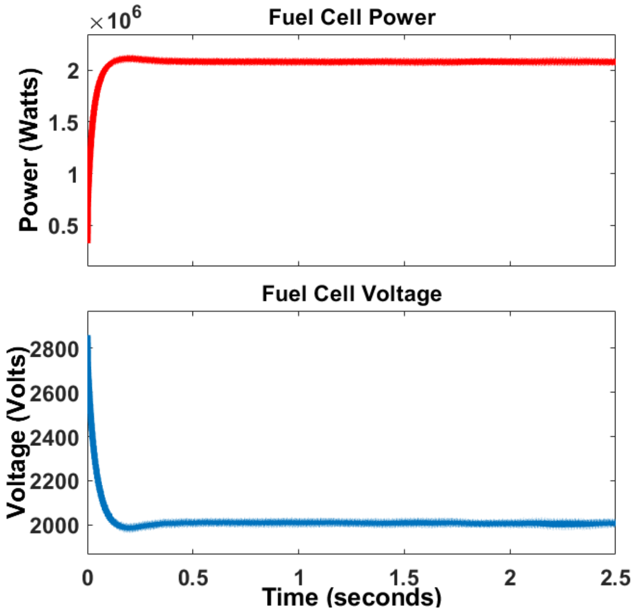

Fig. 4. Fuel cell output power and voltage

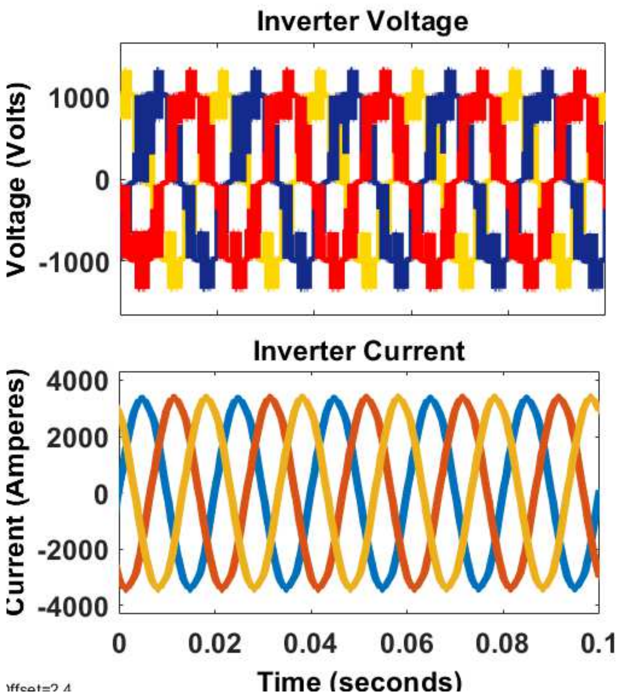

Fig. 5. Inverter voltage and current

The voltage and current of the inverter are shown in Figure 5. The phase-to-phase voltage signal has an RMS value of 938 V, and the phase current is 2384 A. The current wave has fewer harmonics than the voltage wave, as illustrated in Figure 5. The total harmonic distortion of voltage is 52.54 percent at the fundamental frequency of 50 Hz and in the frequency range of 0 to 1000 Hz, while the total harmonic distortion of current is 7.69 percent. THD values obtained may have an impact on the fuel cell, load, and grid, resulting in inefficiencies, low power factors, transients, and other problems.

To eliminate harmonics, an LC filter is installed between the grid (the load) and the inverter. Table V contains the filter parameters. The phase currents and the phase-to-ground voltages at the filter's outputs are shown in Figure 6. The sinewave voltages are 237.8 V, while the currents are around 504.7 A. The voltage overshoot and undershoot measurements are 0.397 and 1.986 percent, respectively. On the other hand, the current overshoot and undershoot were found to be 0.397 percent and 1.986 percent, respectively. The total harmonic distortions of the current and voltage signals at the output of the LC filter are minimal, with 4.86 percent and 2.07 percent, respectively.

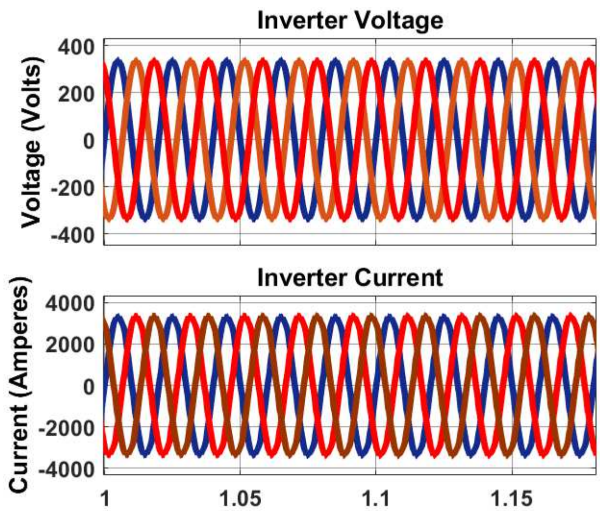

Fig. 6. NPC Inverter voltage and current at filter output terminals

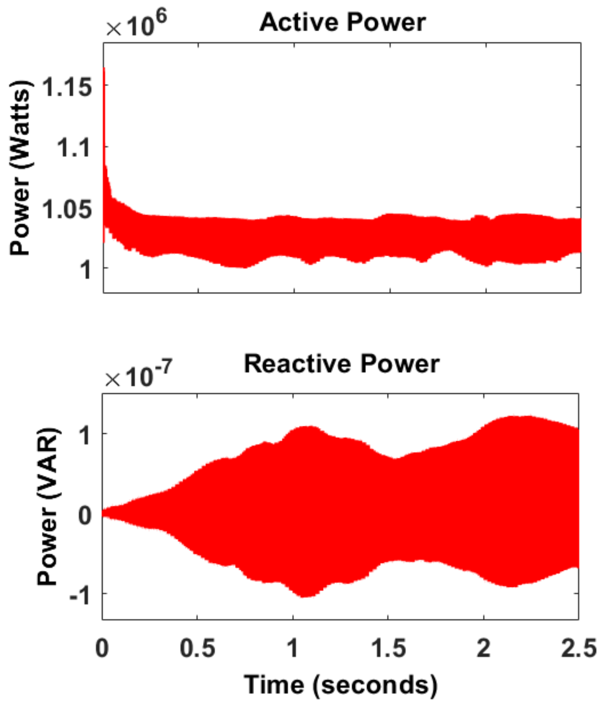

Fig. 7. Load active/Reactive Power

Figure 7 displays the reactive and active power measured at the load terminals of a 1.02 MW localized load connected to the grid-tied inverter's output terminals. The active power in the simulation is 1.025 MW, whereas the reactive power is less than 1 VAR.

The grid-tied fuel cell's surplus power is exported to the grid, and Figure 8 depicts the active and reactive power exported to the grid. The grid receives roughly 696 kW of fuel cell power, with 117 kW of reactive power exported to the grid.

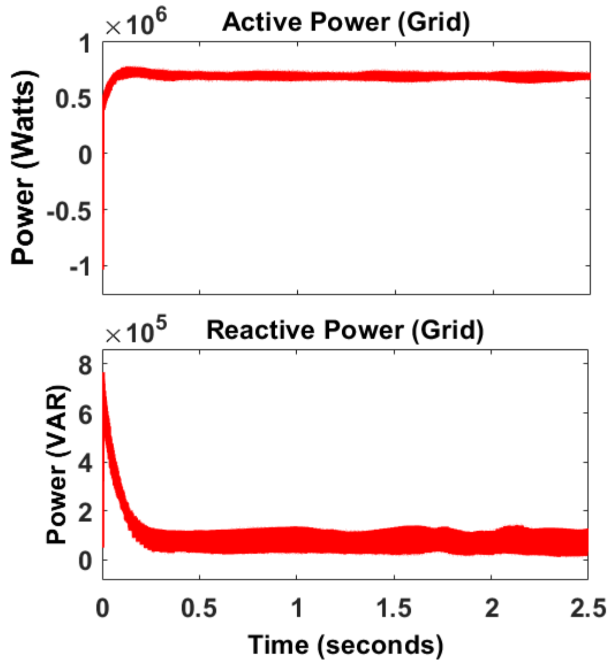

Fig. 8. Grid active/reactive power

IV. Conclusion

Distributed energy resources are significant elements in moving from fossil fuel to green energy systems. Because these power units are increasingly being integrated into existing utility grids, ordinary consumers are now active stakeholders referred to as prosumers. Their capabilities are not limited to consuming electricity but also generating and storing it. If the generation capacity of a prosumer exceeds the load connected to its terminals, there will be a considerable amount of excess electricity. This excess can be sold to neighbouring loads or the utility grid. This study focused on controlling a 2 MW grid-tied fuel cell prosumer. The purpose was to simulate the system, with the inverter operating under a single loop active and reactive power control strategy. A phase-locked-loop was employed to synchronize the fuel cell inverter's frequency and phase with the grid corresponding parameters. Harmonics were mitigated using an LC filter that interfaced with the inverter and the grid. The simulation was carried out in Matlab/Simulink environment. The designed system performed well overall, according to the results. A 1.02 MW local load was connected to the grid-tied fuel cell inverter's output terminals, with 696 kW of extra power exported to the grid.

V. References

[1] J. A. P. Lopes *et al.*, "The future of power systems: Challenges, trends, and upcoming paradigms," *Wiley Interdiscip. Rev. Energy Environ.*, vol. 9, no. 3, pp. 1–16, 2020, doi: 10.1002/wene.368.

[2] C. Zhang, J. Wu, Y. Zhou, M. Cheng, and C. Long, "Peer-to-Peer energy trading in a Microgrid," *Appl. Energy*, vol. 220, no. December 2017, pp. 1–12, 2018, doi: 10.1016/j.apenergy.2018.03.010.

[3] S. Kane, "'Prosumers' have the potential to shift and disrupt the energy landscape," *ESI AFRICA*, 2020. .

[4] K. Ben Hamad, D. N. Luta, and A. K. Raji, "A grid-tied fuel cell multilevel inverter with low harmonic distortions," *Energies*, vol. 14, no. 3, 2021, doi: 10.3390/en14030688.

[5] K. B. Hamad and D. N. Luta, "Pq Open-Loop Control of a Grid-Tied Inverter Interfacing a Large-Scale Fuel Cell Stack," *SSRN Electron. J.*, pp. 1–7, 2021, doi: 10.2139/ssrn.3735393.

[6] X. Wu, G. Tan, Z. Ye, G. Yao, Z. Liu, and G. Liu, "Virtual-Space-Vector PWM for a Three-Level Neutral-Point-Clamped Inverter with Unbalanced DC-Links," *IEEE Trans. Power Electron.*, vol. 33, no. 3, pp. 2630–2642, 2018, doi: 10.1109/TPEL.2017.2692272.

[7] R. G. Shriwastava, M. B. Daigavane, and P. M. Daigavane, "Simulation Analysis of Three Level Diode Clamped Multilevel Inverter Fed PMSM Drive Using Carrier Based Space Vector Pulse Width Modulation (CB-SVPWM)," *Procedia Comput. Sci.*, vol. 79, no. Dcml, pp. 616–623, 2016, doi: 10.1016/j.procs.2016.03.078.

[8] P. Chaturvedi, Shailendra Jain, and Pramod Agrawal, "Modeling, simulation and analysis of three-level neutral point clamped inverter using Matlab/Simulink/power system blockset," no. 2, pp. 1223-1227 Vol. 2, 2008, doi: 10.1109/icems.2005.202742.

[9] K.-B. Lee and J.-S. Lee, *Reliability Improvement Technology for Power Converters*. Singapore: Springer, 2017.

[10] S. Keawthai and S. Po-Ngam, "Simplified Active Power and Reactive Power Control with MPPT and Islanding Detection for Three-Phase Grid-Connected Photovoltaic Inverters," in *ECTI-CON 2015 - 2015 12th International Conference on Electrical Engineering/Electronics, Computer, Telecommunications and Information Technology*, 2015, pp. 8–13, doi: 10.1109/ECTICon.2015.7207035.

[11] Z. Ali, N. Christo, L. Hadjidemetriou, E. Kyriakides, and Y. Yang, "Three-phase phase-locked loop synchronization algorithms for grid-connected renewable energy systems : A review," *Renew. Sustain. Energy Rev.*, vol. 90, pp. 434–452, 2018, doi: 10.1016/j.rser.2018.03.086.

[12] A. Timbus, R. Teodorescu, F. Blaabjerg, and M. Liserre, "Synchronization Methods for Three Phase Distributed Power Generation Systems. An Overview and Evaluation," 2005, doi: 10.1109/PESC.2005.1581980.

[13] X. Buau, X. Wang, D. Pan, D. Yang, W. Li, and C. Bao, "Control Techniques for LCL-Type Grid- Connected Inverters." Springer, p. 319, 2018.

[14] E. Kantar, S. N. Usluer, and A. M. Hava, "Design and performance analysis of a grid connected PWM-VSI system," in *2013 8th International Conference on Electrical and Electronics Engineering (ELECO)*, 2014, vol. 2, pp. 157–161, doi: 10.1109/eleco.2013.6713823.

[15] A. Reznik, M. G. Simoes, A. Al-Durra, and S. M. Muyeen, "LCL Filter design and performance analysis for grid-interconnected systems," *IEEE Trans. Ind. Appl.*, vol. 50, no. 2, pp. 1225–1232, 2014, doi: 10.1109/TIA.2013.2274612.